Surface crack and cracks networks in biaxial fatigue

Alexandre Kane, Véronique Doquet

Surface crack and cracks networks in biaxial fatigue

A. Kane, V. Doquet

Laboratoire de Mécanique des Solides, UMR-CNRS 7649, Ecole Polytechnique, 91128 Palaiseau cedex, France

Semi-elliptical fatigue crack growth in 304 L stainless steel, under biaxial loading, was investigated. Compared to those of through-cracks under uniaxial loading, the growth rate of surface cracks is increased by a non-singular compressive stress and reduced by a tensile stress, when $R = 0$. Plasticity-induced crack closure under biaxial loading was investigated through 3D finite element simulations with node release. Roughness and phase-transformation-induced closure effects were also discussed. The interactions in two-directional crack networks under biaxial tension were investigated numerically. It appears that the presence of orthogonal cracks should not be ignored. The beneficial influence of interaction-induced mode-mixities was highlighted.

Keywords: Surface cracks; Biaxial fatigue; Multiple cracking; Closure effects

1. Introduction

Turbulent mixing of hot (up to 170 °C) and cold (25 °C) water in 304 L stainless steel pipes of nuclear power plants may generate orthogonal networks of thermal fatigue cracks on the inner surface of some pipes (Fig. 1). Even though the steep gradient in thermal stresses combined with shielding effects associated with multiple cracking generally limit in-depth propagation of these cracks, which become quite shallow ($a/c \approx 0.1$ where a and c stand for the depth and surface half-length of the crack, respectively), the risk of through-crack development from such superficial cracks networks has still to be evaluated. Two facets of this complex problem are considered in this study.

* Corresponding author. Tel.: +33 169333355; fax: +33 169333026.
E-mail address: doquet@lms.polytechnique.fr (V. Doquet).

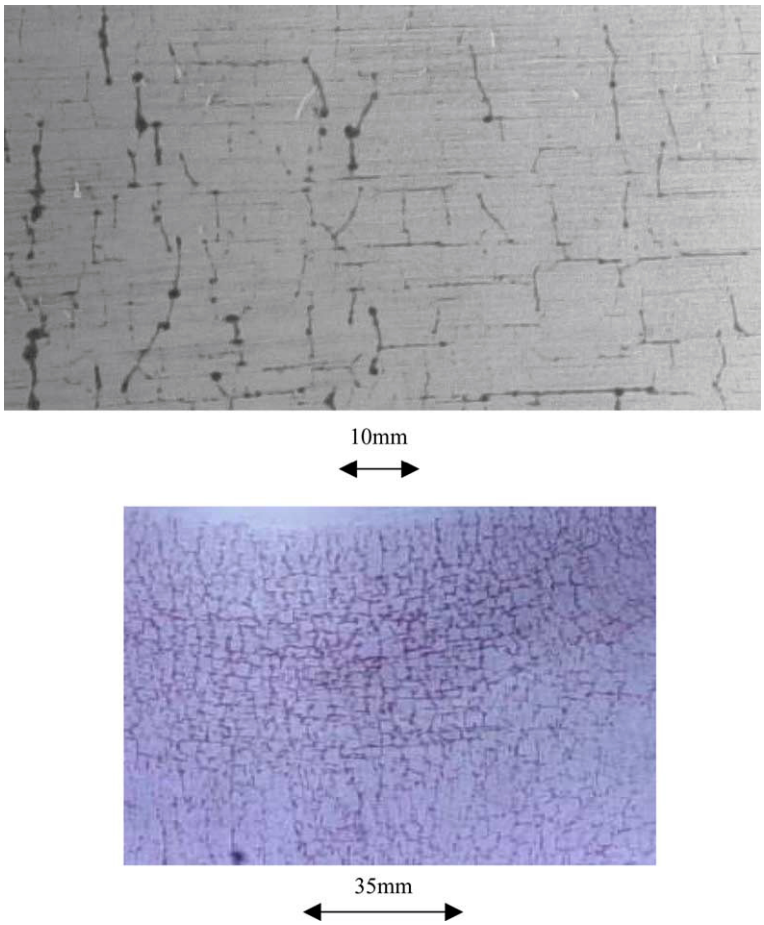

Fig. 1. Typical aspect of thermal cracks network in stainless steel pipes.

To begin with, since thermal loading is biaxial, the cracks growing perpendicular to the first principal stress undergo a likewise stress in their own plane. While many experimental and numerical studies in the literature were devoted to the influence of a non-singular cyclic stress perpendicular to the front of a through-crack in fatigue (see for example [1–3]), few papers (four, to the authors' best knowledge [4–7]) deal with the mode I growth of surface cracks under biaxial loading. A study by Shanyavskii [4] on an aluminium alloy in the striation regime (da/dN between 5×10^{-8} and 2×10^{-6} m/cycle) concludes that, for $R=0.1$, the growth rate of semi-elliptical cracks increases along with $\lambda=\sigma_2/\sigma_1$ (where σ_1 and σ_2 stand for the opening stress and parallel non-singular stress at K_{max}, respectively). Crack flanks interference was thought to explain the deceleration for negative λ. Results obtained with $R=-1$ in the high ΔK regime (da/dN between 10^{-6} and 10^{-5} m/cycle) on 2024 Al alloy by Joshi et al. [5] also suggest that the higher λ, the faster the propagation of surface cracks. By contrast, Kitaoka and Mikuriya [6] found that, for $R=-1$, in the low ΔK range ($da/dN<3\times10^{-8}$ m/cycle), a non-singular compressive stress accelerates crack growth in a carbon steel and that this effect is not rationalized by ΔK_{eff} but by the CTOD, which is increased by a negative λ. Besides, for $R=0$ (and $da/dN<2\times10^{-7}$ m/cycle), Kitaoka and Ohno [7] find almost no influence of biaxiality on mode I surface crack growth in Al_2O_3/Al composites (except in tests where the yield stress was largely exceeded. In those cases, a negative λ reduced da/dN).

So, there are apparently conflicting results in the literature as concerns biaxiality effects, for surface cracks or through-cracks. The only consensus seems to be the absence of any influence of the non-singular stress on surface cracks aspect ratio [4,6,7].

An experimental and numerical investigation of this problem was carried out. Its results constitute the first part of this paper.

The second facet of the problem investigated is related to multiple cracking. Interesting 2D-simulations of multiple fatigue cracking under biaxial loading have been developed by Argence et al. [8], Kullig and Brückner-Foit [9], Hoshide and Socie [10], but such simulations, which consider through-cracks, cannot describe crack arrest due to in-depth stress gradient and are not relevant in the case of pipes superficial thermal cracking. Other existing approaches of the present problem [11,12] consider a through-thickness section of the pipes with edge cracks on the inner surface and either assume plane strain/stress (and straight through-cracks) or an axisymmetric configuration (with circular crack fronts). These models allow only uniaxial loading and parallel edge cracks to be considered, so that only shielding effects are predicted. The overestimate of shielding effects by these models, compared to 3D computations will be discussed. In the present thermal fatigue problem, two sets of mutually perpendicular cracks are often formed. The influence of this second set of cracks has been investigated numerically, in 2D and 3D.

2. Growth of semi-elliptical cracks under biaxial fatigue

2.1. Experimental study

2.1.1. Experimental procedure

The material investigated, 304 L stainless steel ($\sigma_{0.2\%} = 192$ MPa) was supplied as a 30 mm-thick plate. The structure is mainly austenitic except for approximately 3.2% ferrite islands elongated in the rolling direction. The chemical composition is listed in Table 1. This steel is metastable, that is: likely to form strain-induced α' martensite around a crack tip (the Md_{30} temperature, i.e. the temperature for which a tensile strain of 30% transforms 50% of the volume into martensite, deduced from the chemical composition through Angel's empirical equation [13] is 25 °C).

Ten millimeter-thick disks, 100 mm in diameter, with a central semi-elliptical notch parallel to the rolling direction (root radius about 160 μm) and two machined flat zones along the external border, perpendicular to the notch plane were used.

After precracking in diametric compression, two types of fatigue crack growth tests were carried out to investigate the influence of stress biaxiality (Fig. 2).

First, diametric compression tests (Fig. 2a) on disks with notch dimensions: $c = 6$ mm and $a = 3.7$ mm provided data on mode I crack growth in presence of a cyclic compression in the crack plane. The tests were performed at 5 Hz, with constant maximum load and $R = 0.02$. Surface growth rates were obtained from direct crack length measurements with a traveling microscope, while the growth rates in depth are deduced from SEM observations of crack front marks generated by intermittent cycling with $R = 0.5$, keeping K_{max} unmodified. The influence of these intermittent changes in R ratio is believed to be negligible based on the similarity of surface crack growth rates measured just before and just after this change.

Table 1
Chemical composition of 304 L stainless steel (weight percent)

Cr	Ni	Mn	Si	Cu	Mo	N	P	C	S
18.5	10.10	1.13	0.49	0.1	0.09	0.028	0.024	0.023	0.004

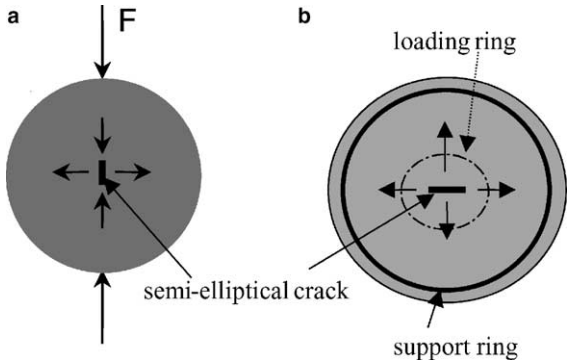

Fig. 2. Principle of semi-elliptical crack growth tests under biaxial loading: (a) diametric compression and (b) biaxial bending.

Second, biaxial bending of similar disks ($c = 5$ mm and $a = 2.5$ mm) supported by a circular ring (radius: 45 mm) and loaded by a smaller concentric circular ring (outer radius 20 mm, width 1 mm) (Fig. 2b) provided data on mode I crack growth with a cyclic tension in the crack plane. For these tests, direct surface crack length measurements were not possible and the specimens were periodically removed from the testing device for surface crack lengths measurements with an optical microscope.

The stress profiles along the crack plane, in the crack-free specimens, computed by FEM for both diametric compression and biaxial bending were plotted on Fig. 3. It appears that in the crack area, the stresses are almost uniform, biaxiality ratios, λ, are -3 and $+1$, respectively.

The maximum opening stress was kept around $\sigma_1/\sigma_{0.2\%} \approx 0.25$ for diametric compression tests and $\sigma_1/\sigma_{0.2\%}$ was progressively increased from 0.38 to 0.78 during the biaxial bending test.

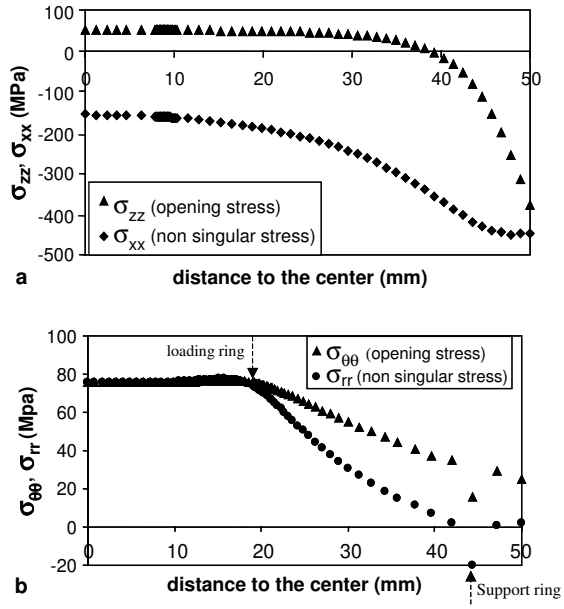

Fig. 3. Profile of principal stresses computed by FEM along a diameter of the crack-free disks: (a) diametric compression and (b) biaxial bending.

Stress intensity factors at the surface and deepest points of the semi-elliptical crack were obtained through 3D finite element computations of J integral, considering one quarter of disk, owing to existing symmetries (Fig. 4a and b). Diametric compression was modelled by a Hertzian pressure distribution on a flat zone along the external border, in the specimen plane, and biaxial bending by a uniform pressure below the loading ring, normal to the specimen plane.

Fig. 4c shows the convergence of the computed SIF at the deepest point with the refinement of the mesh and the uncertainty on the SIF at the free surface, due to the corner point singularity at the free surface. K_I there was in fact computed very near the free surface, just beyond the boundary layer. The SIFs were finally

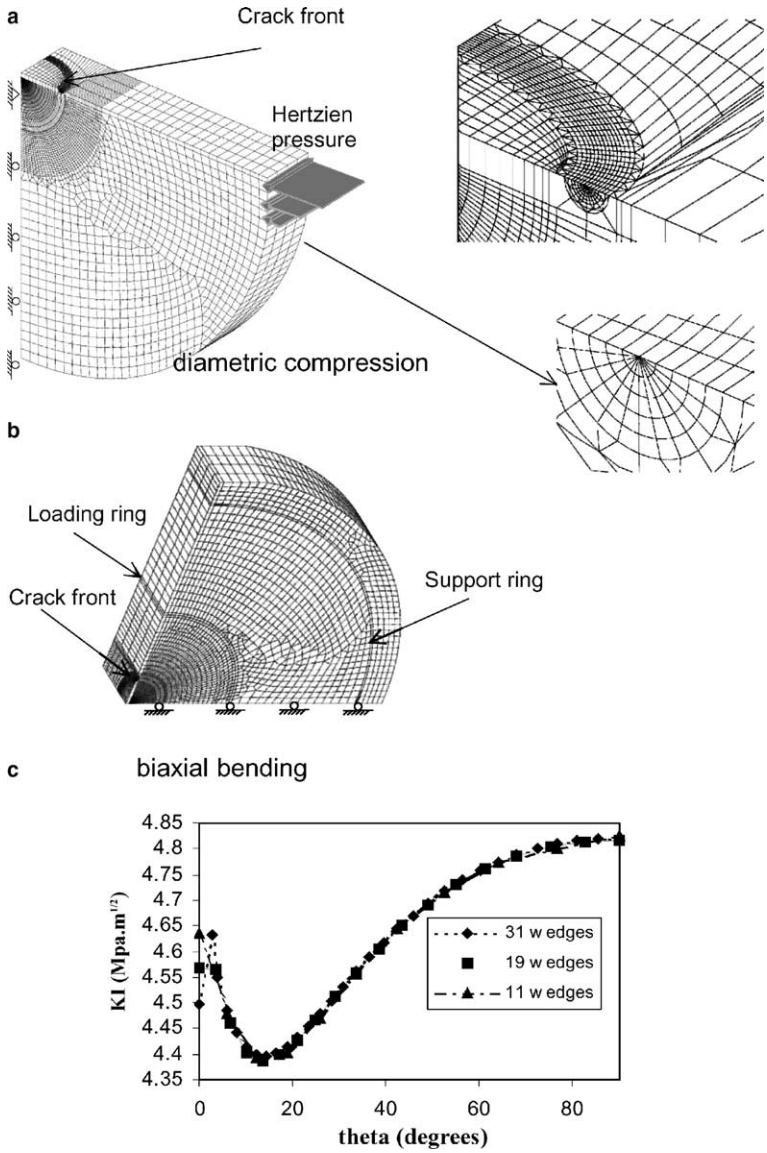

Fig. 4. FEM computation of K_I: (a) diametric compression, (b) biaxial bending, (c) influence of the mesh refinement on K_I computations: convergence of K_I in depth and uncertainty on K_I at the surface due to the corner point singularity.

quite close (within a few percent) to those obtained by inserting the normal stress computed in the crack-free specimens into Raju and Newman's equations [14] for tension and bending in a rectangular plate, but the values used for kinetic data analysis were those issued from our FE simulations.

A clip-on extensometer and, in some specimens, 1 mm-long strain gages straddling the crack at the middle point and just behind one of the crack tips were used to evaluate closure effects. Back-face strain gages were also tested but found not sensitive enough and unreliable. Direct observation of crack faces displacements on smaller specimens (50 mm in diameter, 5 mm thickness, $c = 6$ mm, $a = 3$ mm) precracked, equipped with microgrids (4 μm pitch) and tested in a scanning electron microscope also provided an estimate of $K_{closure}$ (Fig. 5) in diametric compression, at the free surface.

2.1.2. Experimental results

In diametric compression, an initial deceleration during the first millimeter of crack growth, followed by normal evolution of da/dN with ΔK_I was observed, at the surface as well as in depth (Fig. 6a). In biaxial bending, a similar transient deceleration was observed, at the surface, but at the deepest point, the growth rate continuously dropped. A 3D elastic–plastic FEM analysis in which both the crack and notch were modelled was made and K_I at the crack tip was computed by fitting the opening stress profiles ahead of the crack front in the K-dominance zone. No decrease in ΔK_I, which could have explained the observed deceleration was obtained for the corresponding crack dimensions, so that the transient deceleration was not due to a notch effect. The deceleration was thus a "small-crack-like" effect, due to an increase in closure load. Song and Shieh [15] recently reported a similar effect during the first 3 mm of propagation of surface cracks in AISI 4130 steel.

In diametric compression, beyond the first millimeter of crack growth, in situ observations and COD measurements both yielded $K_{closure}/K_{max} = 0.3 \pm 0.03$ and this value was thus used for closure correction, at the surface.

In biaxial bending, the clip-on extensometer, and the strain gage glued across the notch, in the middle point both indicate $K_{closure}/K_{max} < 0.15$, whereas a strain gage glued across the crack, just behind one of the tips yielded $K_{closure}/K_{max} = 0.5$.

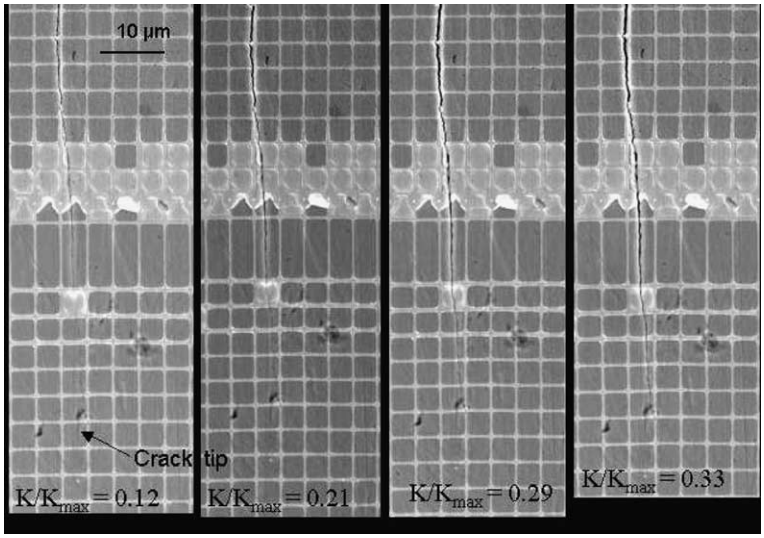

Fig. 5. Estimation of $K_{closure}$ at the free surface by direct observation of crack flanks displacements while loading a specimen in diametric compression in the SEM (pitch of the grids: 4 μm).

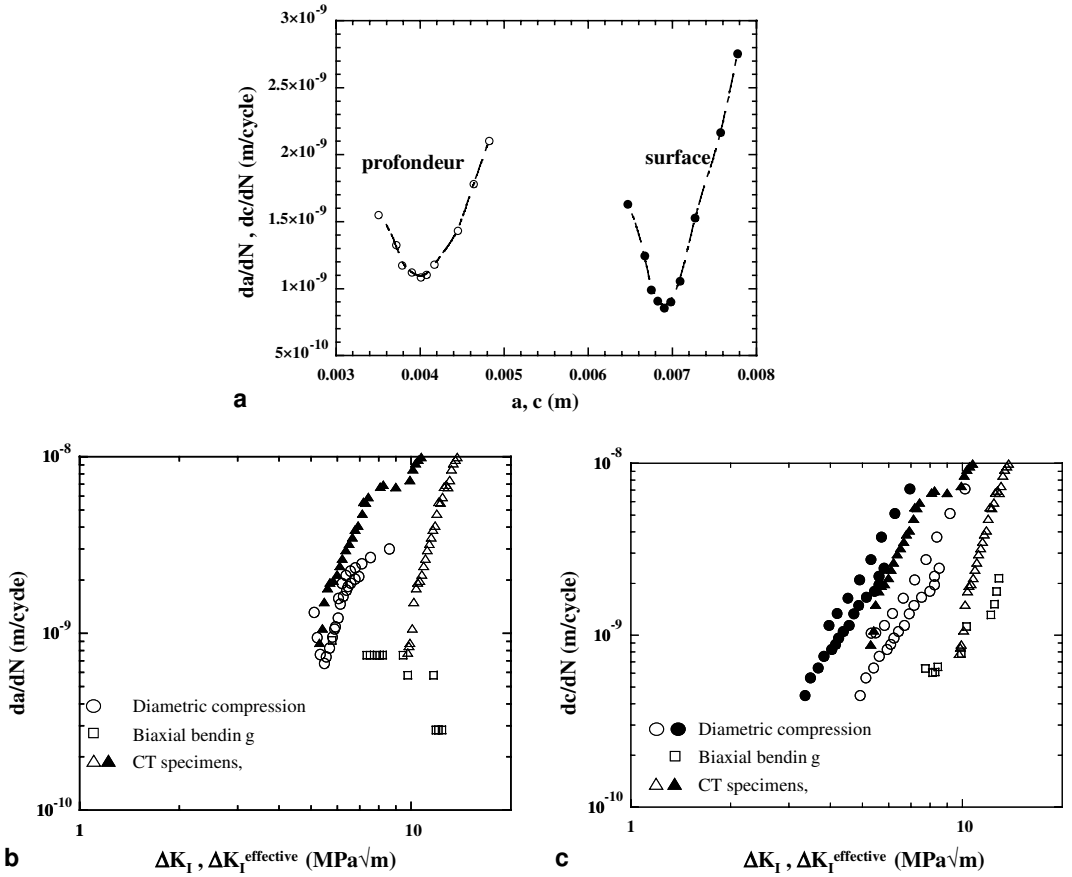

Fig. 6. Crack growth kinetics measured in diametric compression, biaxial bending (a) transient deceleration, (b) and (c) comparison of kinetic data collected at the deepest point and surface points of semi-elliptical cracks, respectively, to data from CT specimens (open symbols: nominal ΔK, black symbols: effective ΔK).

The surface crack growth rates measured at the surface and in depth were plotted on Fig. 6b and c, respectively, together with data obtained, on the same batch of steel for through-cracks in CT specimens at $R = 0$. In the latter case, crack opening was monitored by a crack-mouth extensometer and K_{closure} was deduced from the analysis of the force versus crack opening curve. The evolution of $\mathrm{d}a/\mathrm{d}N$ versus ΔK_{I} in depth, for biaxial bending is quite unusual. A tentative explanation is proposed below.

Despite some scatter in data, it seems that compared to the growth of through-cracks under uniaxial loading, the growth of semi-elliptical cracks is faster in diametric compression and slower in biaxial bending, for the same nominal ΔK.

SEM fractographic observations revealed no striations, in accordance with the small ΔK_{I} range investigated. Lamellar patterns suggest some strain-induced martensitic transformation (Fig. 7a). Furthermore, areas close to fracture surfaces become magnetic.

Signs of friction could be observed on some areas of specimens tested in diametric compression (Fig. 7b), which recalls Shaniavskii's observations of enhanced crack flanks interactions when a compressive stress is applied in the crack plane [4].

Such signs were not found on specimens tested in biaxial bending, characterised by a higher roughness (Fig. 7c), secondary cracks, more or less perpendicular to the non-singular tensile stress a more brittle

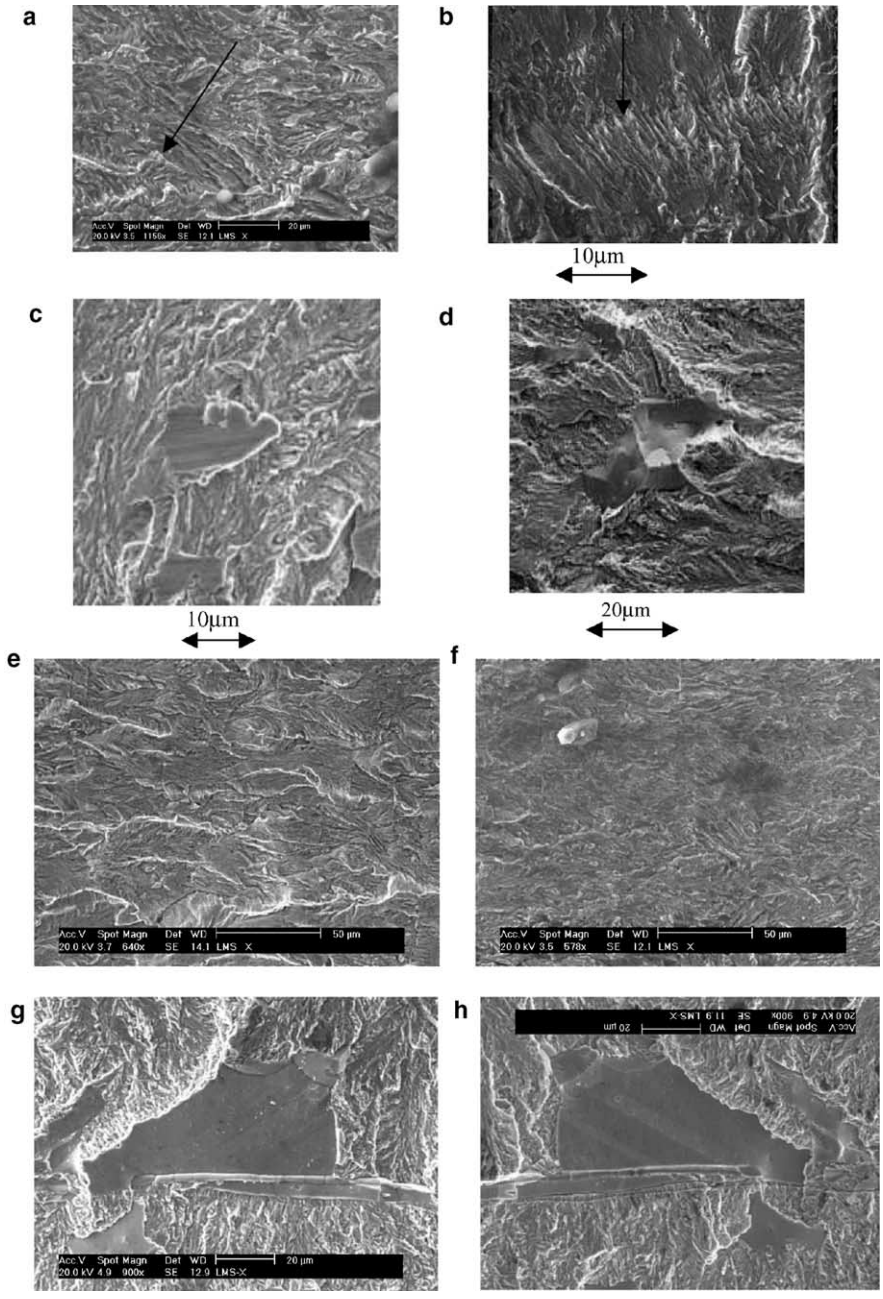

Fig. 7. Typical aspect of fracture surfaces: (a and b) lamellar patterns evoking broken martensite, (c) zone mated by friction in diametric compression (d) brittle-like facets in biaxial bending, (d and e) comparison of fracture surfaces in biaxial bending (d) and diametric compression (e), (g and h) comparison of matching areas on both fracture surfaces in biaxial bending.

aspect and cleavage facets (Fig. 7d–f) as evidenced by the similarity of details on mating zones of the two fracture surfaces (Fig. 7e and f), which excludes intergranular decohesion. Since the austenitic phase does not, in principle, exhibit cleavage, these facets most probably correspond to ferrite islands. The distribution

of cleavage facets is not uniform on the fracture surface: they are more frequent in areas corresponding to higher ΔK, at the surface as well as in depth.

Tanaka et al. [2] also reported brittle-like facets and many secondary cracks in biaxial tension and Bethge et al. [17], who studied crack propagation due to thermal fatigue (a biaxial tension stress state as well) in a pressure vessel steel similarly report rougher fracture surfaces than under uniaxial mechanical loading and plenty of secondary cracks.

To get an objective evaluation of fracture surface roughness, topographic 3D maps of selected areas on fracture surfaces (along the in-depth and surface crack growth directions) were deduced from series of 80 to 100 optical microscope digital images (2048×2048 pixels) taken at 1 μm intervals in vertical distance. When a zone is in-focus, the local contrast, characterized by the ratio of local variance of gray levels to local average gray level is highest. A procedure searching, for each pixel, the altitude corresponding to the maximum local contrast was developed and used to reconstruct a 3D image of fracture surfaces. After correction for mean plane inclination, the resulting topographic maps were used for roughness evaluation. A discretization of the fracture surface into small triangles was made and roughness was computed as the sum of triangles areas divided by the total projected area [16]. The measurements were made for diametric compression and biaxial bending, in 150 μm × 500 μm zones corresponding to similar ranges of ΔK_I, along the in-depth and surface crack growth directions. The results gathered in Table 2 show that fracture surfaces roughness is higher in biaxial bending than in diametric compression, at the surface as well as at the deepest point, which confirms the visual impression.

2.2. Numerical study

A numerical evaluation of closure effects along the front of a semi-elliptical crack under biaxial loading was attempted through elastic–plastic finite element simulations with periodic node release to simulate crack growth and plastic wake formation. A similar procedure has been developed in 3D FEM by various authors [18–21] but only for uniaxial loading.

Elastic–plastic constitutive equations with isotropic and non-linear kinematic hardening were fitted to experimental stress–strain curves for 316 L stainless steel.

The flow criterion and flow rule—where J_2 denotes the second invariant of the stress deviator, $\underline{\underline{X}}_1$ and $\underline{\underline{X}}_2$ two non-linear kinematic hardening variables and R an isotropic hardening variable are:

$$f = J_2(\underline{\underline{\sigma}} - \underline{\underline{X}}_1 - \underline{\underline{X}}_2) - R = 0, \quad \mathrm{d}f = 0 \tag{1}$$

$$\dot{\underline{\underline{X}}}_i = C_i \dot{\underline{\underline{\varepsilon}}}_p - \gamma_i \underline{\underline{X}}\, \dot{p}, \quad i = 1, 2 \tag{2}$$

where $\dot{p} = \sqrt{\frac{2}{3}\dot{\underline{\underline{\varepsilon}}}_{vp} : \dot{\underline{\underline{\varepsilon}}}_{vp}}$ is the equivalent plastic strain rate and C_1, C_2, γ_1, γ_2 are constants.

$$R = k_0 + Q(1 - \exp(-b \cdot p)) \tag{3}$$

where k_0 (initial yield stress) and Q are constants.

Table 2
Results of fracture surface roughness evaluations (ΔK_I values correspond to the area on the fracture surface where the roughness value reported in the previous column were obtained)

	Rs surface	ΔK_I (MPa$\sqrt{m}$)	Rs depth	ΔK_I (MPa$\sqrt{m}$)
Diametric compression	1.49	6–7	1.33	6.9–7.5
Biaxial bending	2.19	5–5.6	2.78	8.1–9.9

Table 3
Material constants used in constitutive equations

E (MPa)	k_0 (MPa)	b	Q (MPa)	C_1 (MPa)	γ_1	C_2 (MPa)	γ_2
194,500	185	3.85	200	22,400	40	40,000	1000

$$\dot{\underline{\underline{\varepsilon}}}_p = \alpha \frac{\partial f}{\partial \underline{\underline{\sigma}}} \tag{4}$$

where α is determined from (1)–(3). The material constants in (1)–(4) are gathered in Table 3.

A semi-elliptical crack ($a/c = 0.5$) in a plate with finite thickness, t, but "infinite" height and width was considered. It was submitted to either an opening stress σ alone or opening stress plus tension or compression $\pm\,\sigma$ parallel to the free surface (that is: $\lambda = 0$, 1 or -1, the latter equivalent to a shear stress field). The crack aspect ratio was kept constant during node release. Past the first cycle, one element was released at each subsequent cycle, at K_{max} (Fig. 8a). During crack "propagation", the a/t ratio varied from 0.1 to $\approx$0.106. Fig. 8b shows the mesh used for all biaxiality ratios. There were at least ten linear elements (with equal height and width) in the initial plastic zone ahead of the crack front. $K_{closure}$ corresponds to the load for which the opening displacement of the first node behind the crack front became negligible at unloading. Unilateral contact conditions were enforced to avoid crack surface interpenetration. The simulations have been performed for $R = 0$, -0.5 and -1. The applied stress level, σ, was varied from 16% to 54% of the micro-yield stress, k_0, so that small-scale yielding conditions prevailed, even when the stress parallel to the crack was compressive.

Fig. 9a, compares the computed evolution of $K_{closure}/K_{max}$ at the free surface and in depth, for the three loading cases considered for $\sigma = 0.54\sigma_y$ and $R = 0$, as the crack propagates. Fig. 9b and c shows the steady-

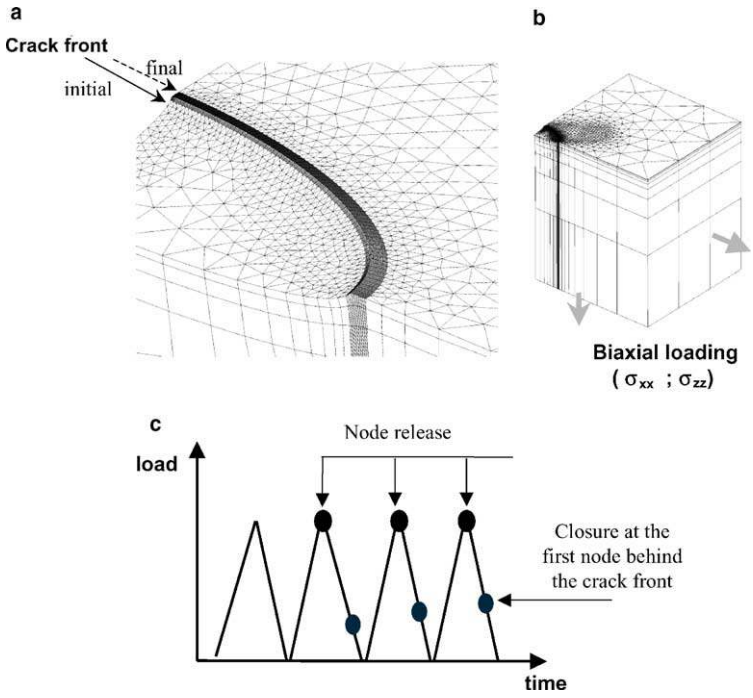

Fig. 8. (a) and (b) Finite element mesh and (c) procedure used to evaluate $K_{closure}$.

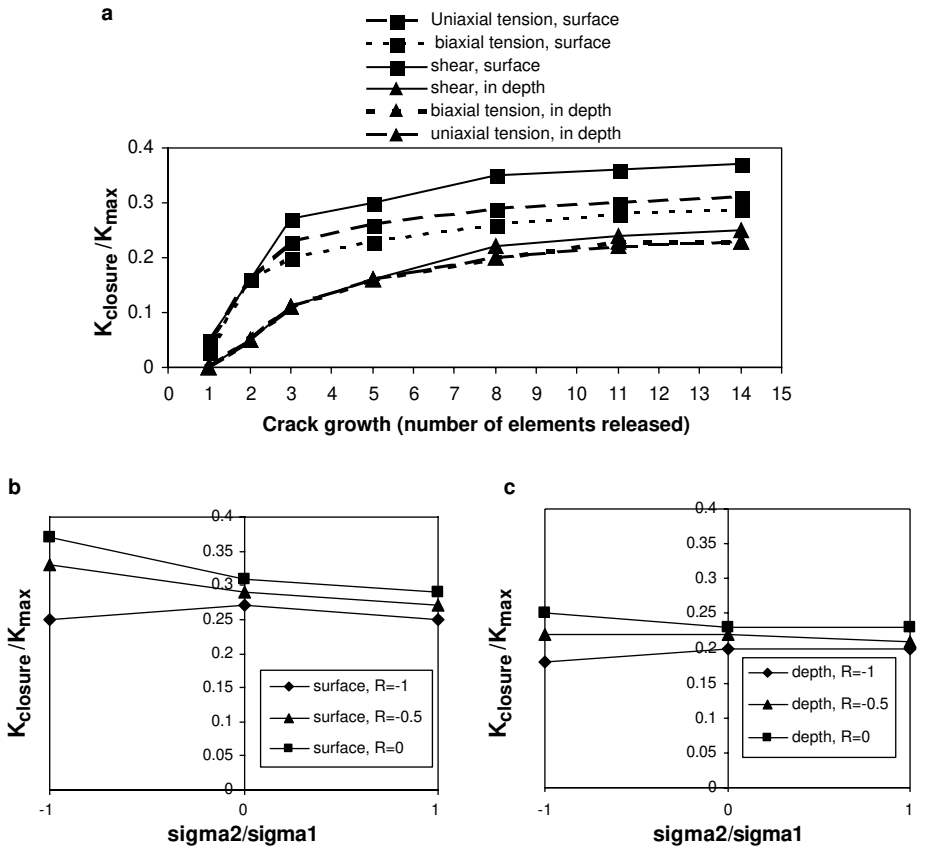

Fig. 9. Influence of load biaxiality on plasticity-induced crack closure for a semi-elliptical crack in a finite-thickness plate ($a/c = 0.5$, $a/t = 0.1$–0.106, $\sigma_{max}/\sigma_y = 0.54$). (a) Computed evolutions of $K_{closure}/K_{max}$ with crack growth for uniaxial, shear and equibiaxial loadings. Steady-state $K_{closure}/K_{max}$ as a function of biaxiality, for various R ratios (b) at the surface and (c) at the deepest point.

state $K_{closure}/K_{max}$ as a function of remote biaxiality, for the three R ratios, at the surface and at the deepest point, respectively.

In accordance with previous numerical studies [17–20], closure is more pronounced at the free surface ($K_{closure}/K_{max}$ ranges from 0.25 to 0.37, depending on R ratio) than in depth ($K_{closure}/K_{max}$ ranges from 0.18 to 0.23), because crack tip plasticity is more widespread in plane stress than in plane strain.

In-depth closure does not seem to be modified by a non-singular tensile stress whatever the R ratio, but it is either raised or decreased by a non-singular compressive stress, depending on R.

At the surface, for $R = 0$ and -0.5, closure was predicted to be highest in shear ($K_{closure}/K_{max} = 0.37$) and smallest in equibiaxial tension ($K_{closure}/K_{max} = 0.29$), which is consistent with experimental results by Shaniavskii [4] (fastest crack propagation in biaxial tension, slowest in shear, when $R = 0$).

For $R = -1$, a non-singular compressive stress was predicted to slightly reduce closure compared to uniaxial loading, at the surface ($K_{closure}/K_{max} = 0.25$ instead of 0.27) as well as in depth ($K_{closure}/K_{max} = 0.18$ instead of 0.2).

To investigate a possible influence of load biaxiality on crack aspect ratios, the ratio of effective $\Delta K = K_{max} - K_{closure}$ at the free surface and in depth has been computed:

Table 4
Comparison of effective ΔK at the surface and in depth

$\Delta K_{surface}^{effective}/\Delta K_{depth}^{effective}$	Shear	Uniaxial tension	Equibiaxial tension
$R=0$	0.84	0.90	0.92
$R=-0.5$	0.86	0.91	0.92
$R=-1$	0.91	0.91	0.94

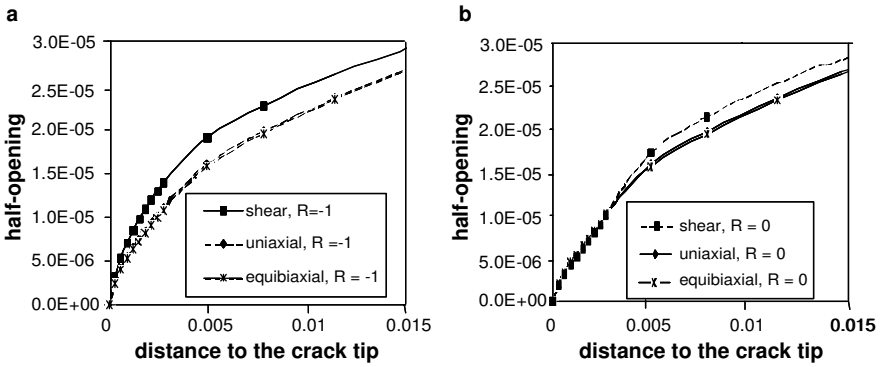

Fig. 10. Comparison of steady-state near-tip opening profiles at the surface of a semi-elliptical crack computed at K_{max} (a) for $R=-1$, (b) $R=0$.

$$\frac{\Delta K_{surface}^{eff}}{\Delta K_{depth}^{eff}}=\frac{K_{max,surface}\left(1-\frac{K_{closure,surface}}{K_{max,surface}}\right)}{K_{max,depth}\left(1-\frac{K_{closure,depth}}{K_{max,depth}}\right)}$$

The results gathered in Table 4 (where the ratio of K_{max} values at the surface and depth, which does not vary with biaxiality was taken equal to one) show less than 10% variation when biaxiality changes, so that the crack aspect ratio should not depend on the type of loading. This is consistent with experimental observations by Shaniavskii [4] and Kitaoka et al. [6].

Kitaoka and Mikuriya [6] found that the influence of load biaxiality on surface crack growth is not well rationalized by ΔK^{eff} but much better by ΔCTOD. The influence of load biaxiality on steady-state near-tip opening profiles computed at K_{max} at the free surface has thus been examined (since the minimum COD is zero, close to the tip, the amplitude, ΔCTOD is equal to the maximum CTOD). Fig. 10 shows that for $R=-1$, the maximum opening is significantly increased by a non-singular compressive stress, while for $R=0$, the near-tip opening is the same whatever the biaxiality. These two results are perfectly consistent with the measurements by Kitaoka and Mikuriya.

3. Discussion

Ogura et al. [22] as well as McClung [3] had performed finite element simulations of through-cracks propagation in plane stress and shown that for $R=-1$, a compressive stress in the crack plane decreases plasticity-induced crack closure, while a tensile stress has the reverse effect, which was consistent with the acceleration or deceleration of crack growth observed, in corresponding cases, by Tanaka et al. [2] and Miller et al. [1] when $R=-1$.

When $R = 0$ however, Tanaka et al. [2] observed that a compressive stress in the crack plane reduced the crack growth rate. Simulations performed by Ogura et al. [22] for $R = 0$, in plane stress yielded slightly more closure effects in shear than under uniaxial or equibiaxial loadings. This tendency was thus reversed compared to $R = -1$ but coherent with the experimental results by Tanaka et al. [2].

Fleck and Newman [23] computed the COD of propagating fatigue cracks in two specimens with either positive or negative T stress, in plane strain, and showed (Fig. 13 of [23]) that for $R = 0$, a negative T stress, does not change ΔCOD, but that it increases $K_{closure}/K_{max}$, for $R = -1$. So, literature suggests that biaxiality effects do depend on the R ratio and the present results go in the same sense.

But unfortunately, finite element simulations can capture only plasticity-induced closure effects, whereas roughness-induced closure as well as phase-transformation-induced closure might play an important role in the present case.

Cotterell and Rice [24] have shown that when there is a negative T stress perpendicular to a crack front, an incipient tilted branch crack tends to turn back to the main crack plane whereas any perturbation of the crack path is amplified when a positive T stress is present. This suggests a possible influence of load biaxiality on fatigue crack roughness and thus roughness-induced closure, since variations in remote biaxiality will modify the local T stress.

Wang [25,26] recently provided expressions for the T stress around a semi-elliptical crack in a finite thickness plate subjected to non-uniform uniaxial stress distributions and explained how to use a superposition principle to compute T for more complex loadings. In the present case, remote load biaxiality modifies the T stress at the surface but not in depth. Using Wang's equations, it can be shown that during diametric compression tests, the T stress at the surface is approximately -200 MPa, while in biaxial bending, it varies from $+65$ to $+192$ MPa as the crack propagates. This might partly explain why the roughness of the fracture surfaces close to the free surface is higher in biaxial bending than in diametric compression and why crack propagation is slower.

The sign of the T stress at the deepest point does not change with load biaxiality (-30 to -40 MPa in diametric compression versus -35 to -70 MPa in biaxial bending), but at that point, there is also a non-singular stress parallel to the crack front.

Such a stress does not exist in 2D, so that very few information could be found in the literature about its possible influence. Xu et al. [27] predicted that the influence of this kind of non-singular stress on twisted branch cracks would be similar to the influence of the "classical" T stress on tilted branch cracks, that is: a tensile (respectively compressive) stress parallel to the crack front might favor (respectively inhibit) crack twisting. This would explain our observations concerning the high number of secondary cracks more or less perpendicular to the applied tensile stress. These secondary cracks could shield the main crack tip and be partly responsible for the continuous deceleration of in-depth propagation under biaxial tension.

In addition, in this metastable 304 stainless, α' martensite is probably formed around the crack tip. Mei and Morris [28,29] have shown that the volume expansion associated with this martensitic transformation (approximately 2%) generates closure effects in fatigue, intrinsically difficult to measure however, due to an unusual variation of the COD with the applied stress. Stringfellow et al. [30] as well as Tomita et al. [31] have developed constitutive models for such metastable steels in which the volume fraction of strain-induced martensite increases with the stress triaxiality ratio.

The triaxiality ratio just ahead of the front of a semi-elliptical crack ($a/c = 0.5$) in a plate with thickness t has thus been computed by FEM, in elasticity, for remote biaxiality ratios λ equal to -3 and $+1$. The results were gathered in Table 5. A tensile stress in the crack plane increases triaxiality, while a compressive stress decreases it and the effect is more pronounced at the deepest point than at the surface. A higher martensite volume fraction might thus be expected to form under biaxial bending than under diametric compression, especially at the deepest point. This might partly explain the continuous deceleration of in-depth crack propagation under biaxial bending. X-ray measurements of martensite volume fraction around the crack plane will be performed to check the validity of this assumption.

Table 5
Triaxiality ratios just ahead of the front of a semi-elliptical crack ($a/c = 0.5$) in a plate of thickness t

a/t	Diametric compression surface	Diametric compression depth	Biaxial bending surface	Biaxial bending depth
0.1	0.28	0.51	0.79	1.42
0.5	0.14	0.35	0.66	1.03
0.8	0.23	0.28	0.65	0.62

3.1. Interaction of orthogonal crack networks under biaxial tension

Existing approaches of the present problem [11,12] consider a through-thickness section of the pipes with edge cracks on the inner surface and either assume plane strain/stress (and straight through-cracks) or axisymmetric configuration (with circular crack fronts). The conservatism of such approaches can be questioned.

On the one hand, for an isolated crack, 2D or axisymmetric computations overestimate K_I, compared to its value at the deepest point of a semi-elliptical crack, by a factor that increases with the crack aspect ratio, a/c. But, on the other hand, it was shown by Isida et al. [32] that shielding interactions between stacked parallel cracks computed in 2D (plane strain) are quite exaggerated compared to those obtained in 3D, so that the safety margin associated with a straight through-crack approximation can be reduced to zero as the distance between parallel cracks decreases (see Fig. 11, which shows that the computed K_I are still higher than in 3D, but the difference with a 3D computation is much less than for an isolated crack and decreases as parallel cracks get closer). The results of axisymmetric computations performed in the present study were also plotted. Such an approach also overestimates shielding effects, but to a lesser extent than a plane strain approach and should thus be preferred, in the present case.

In addition, when a through-thickness section of the pipes with edge cracks is modelled, only parallel cracks can be considered. However, in the present thermal fatigue problem, two sets of mutually perpendicular cracks are often formed and, under biaxial tension, orthogonal cracks may, as shown below amplify crack tip singularities.

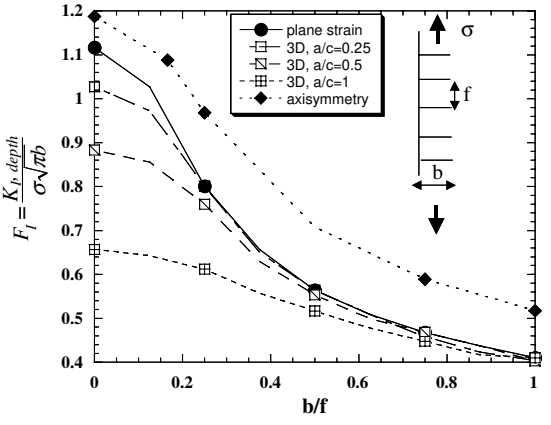

Fig. 11. Stress intensity factor ($F_I = \frac{K_{I,depth}}{\sigma\sqrt{\pi b}}$) at the deepest point of periodically stacked similar surface cracks under tension as a function of their relative spacing, in 2D (plane strain), axial symmetry (circular crack fronts) or 3D (semi-elliptical cracks, from Isida et al. [32]).

FE elastic computations of stress intensity factors under equibiaxial tension were performed for two perpendicular semi-elliptical cracks of equal length $2c$ and aspect ratio $a/c = 0.5$ in a finite thickness plate ($a/t = 0.25$). The vertical crack plane was kept at a distance $x = 0.18c$ from the rightmost tip of the horizontal crack and the altitude of its center was varied. K_I values computed on the closest surface points as well as at the deepest point were normalised by K_I for the isolated crack and plotted versus y/c on Fig. 12. An amplification effect (up to 10% increase in K_I compared to an isolated crack) was found when one tip of the vertical crack was in the plane of the horizontal crack. This amplification is not negligible since for low ΔK, it could make the difference between propagation and arrest and for mid-range ΔK, with a Paris exponent around 4, such an amplification would lead, approximately, to a 40% increase in the growth rate. If a through-thickness section of the pipes with only parallel edge cracks is modelled (either in 2D or axisymmetry) this amplification cannot be taken into account and predictions of remaining fatigue lives can become non-conservative.

An orthogonal network of 19 cracks, was also considered (Fig. 13) and SIFs were computed on each of the 38 tips, either taking into account the whole network, or considering only the parallel cracks sub-network (in order to estimate the error due to the latter procedure). Fig. 13a shows the amplification or shielding effect of parallel and orthogonal networks on K_I. A majority of crack tips are shielded (the average normalised K_I are 0.75/0.787 for parallel/respectively orthogonal network) but amplification occurs for 25–30% of the crack tips (either crack tips on the border of the cracked zone, due to less shielding plus a kind of "load transfer" effect, or parallel coplanar cracks, or cracks with an orthogonal neighbour). Such amplifications would not be described if a through-thickness section had been considered.

The average ratio of K_I in the biaxial crack network to K_I in the parallel sub-network for each individual crack tip is 1.39. Ignoring the second set of cracks would thus lead to underestimate K_I and thus to

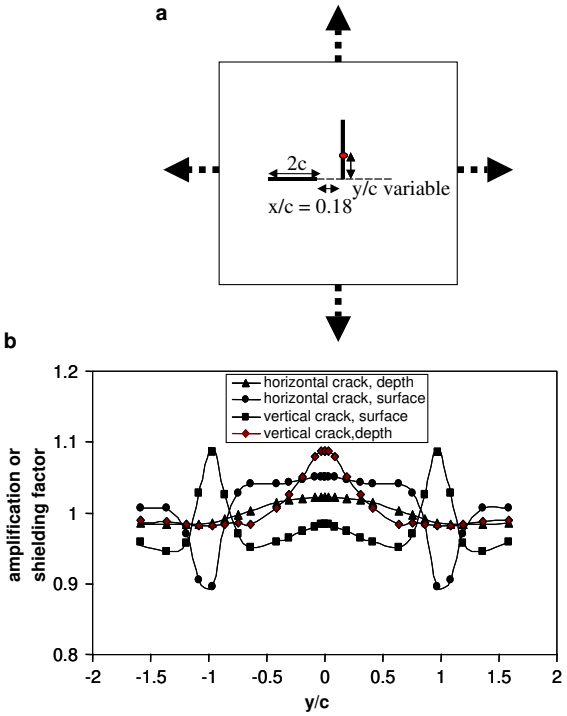

Fig. 12. Interaction between two identical orthogonal semi-elliptical cracks under equibiaxial tension. (a) Cracks configuration, (b) amplification or shielding factors ($a/c = 0.5$, $a/t = 0.25$).

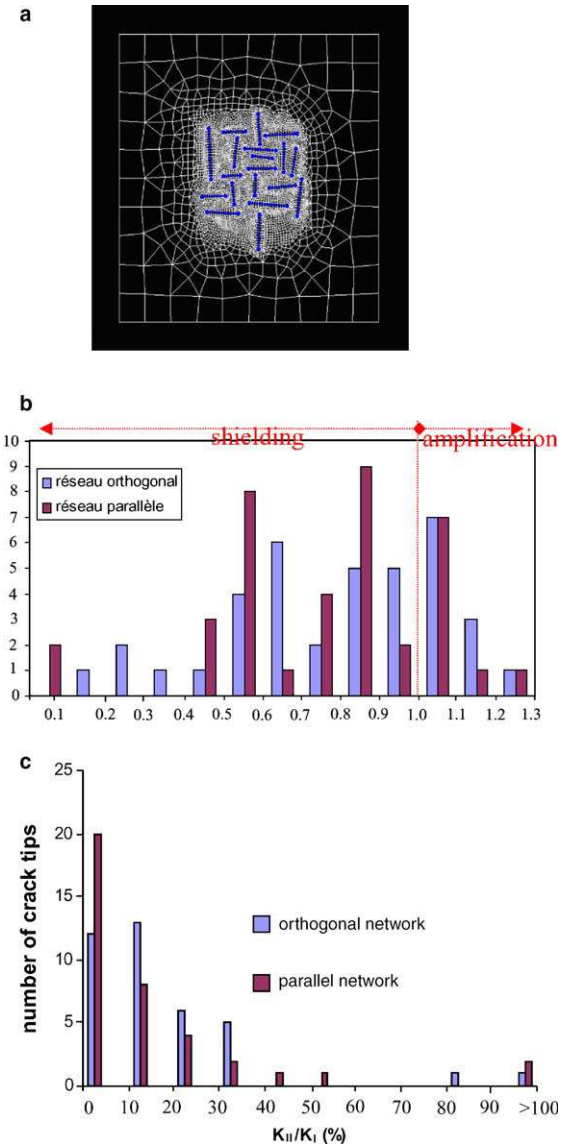

Fig. 13. Interactions in an orthogonal crack network in equibiaxial tension. (a) Network of 19 cracks considered, (b) distribution of K_I, (c) distribution of the mode-mixity ratios for the 38 crack tips.

non-conservative predictions of the remaining life (not to mention the fact that orthogonal cracks are likely to induce coalescence between parallel cracks that would otherwise be too far away to interact and link).

Fig. 13b shows the mode-mixity ratio, K_{II}/K_I, computed for each of the 38 crack tips, either in the orthogonal network or in the parallel sub-network. This ratio exceeds 20% for many cracks, which implies their bifurcation by more than 29°. The beneficial influence of multiple cracking, generally attributed merely to shielding effects has an additional origin: crack path roughness due to repeated bifurcations should reduce the crack growth rates because of asperity-induced closure.

Simulations of semi-elliptical cracks network development based on 3D FE computations, which would allow consideration of thermal stress gradients in depth as well as of orthogonal networks can be envisaged only for a limited number of cracks and it would be difficult to take bifurcations and crack roughness into account. Anyway, since crack roughness has a beneficial impact on the fatigue life, such simulations, considering only mode I growth of plane 3D cracks would be conservative. The Extended Finite Element method (XFEM [33]), which can be used for a large number of cracks [34] might provide an alternative approach of thermal fatigue cracking in the future.

4. Conclusions

- The influence of load biaxiality on mode I propagation of surface cracks in 304 L stainless steel has been investigated through diametric compression tests and biaxial bending tests. Compared to the growth of through-cracks under uniaxial loading, the growth of semi-elliptical cracks for $R = 0$ is faster in diametric compression and slower in biaxial bending, for the same nominal ΔK_I.
- Fracture surfaces formed under biaxial bending were quite rough, with secondary cracks and cleavage facets in the ferrite phase. An explanation based on increased stress triaxiality and crack path stability reduction by the positive T stress, at the surface and the non-singular stress parallel to the crack front, in depth, was proposed.
- The influence of load biaxiality on plasticity-induced closure along the front of a semi-elliptical crack under biaxial loading was investigated through elastic–plastic finite element simulations with periodic node release. In-depth, closure is not modified by a non-singular tensile stress whatever the R ratio, but it is either raised or decreased by a non-singular compressive stress, depending on R. At the surface, for $R = 0$ and $R = -0.5$, closure was predicted to be highest in shear and smallest in equibiaxial tension, but for $R = -1$, it is smallest in shear. The ratio of effective ΔK at the free surface and in depth is almost unchanged, whatever the biaxiality, for a given R ratio, so that fatigue cracks aspect ratio should not depend on the type of loading.
- In the metastable 304 L stainless steel, strain-induced α' martensite was probably formed around the crack tip. Its volume fraction, and thus the importance of induced closure effects probably vary with load biaxiality. This point deserves further investigation.
- Shielding interactions between stacked parallel cracks computed either in 2D or for an axisymmetric configuration are exaggerated compared to those obtained in 3D, so that the safety margin associated with a straight through-crack approximation can be strongly reduced as the distance between parallel cracks decreases. However, the overestimate of shielding effects is less important in axisymmetric computations, so that this approach should be preferred, in the present case.
- 3D elastic FE simulations show that under biaxial tension, the presence of a second population of orthogonal cracks amplify crack tip singularities. This effect cannot be captured if a through-thickness section of the pipes with only stacked parallel cracks is considered.
- In a dense crack network, interaction-induced mode mixity ratios are high and responsible for repeated bifurcations. The beneficial influence of multiple cracking is thus partly due to increased crack roughness and asperity-induced closure.

Acknowledgements

Financial support for his study is provided by EDF. Kinetic data for through-cracks in CT specimens was kindly provided by J.C. Leroux, from EDF/DER/EMA.

References

[1] Miller KJ, Brown MW. Mode I fatigue crack growth under biaxial stress at room and elevated temperature. In: Miller KJ, Brown MW, editors. Multiaxial fatigue. ASTM STP 853. Philadelphia: ASTM; 1985. p. 135–52.

[2] Tanaka K, Hoshide T, Yamada Y, Taira S. Fatigue crack propagation in biaxial stress fields. Fat Fract Engng Mater Struct 1979;2:181–94.

[3] Mc Clung RC. Closure and growth of mode I cracks in biaxial fatigue. Fat Fract Engng Mater Struct 1989;5:447–60.

[4] Shanyavskii AA. Development of semi-elliptical fatigue cracks in AK6 aluminium alloy under biaxial loading. Fat Fract Engng Mater Struct 1996;19(12):1445–58.

[5] Joshi SR, Shewchuk J. Fatigue crack propagation in a biaxial stress field. Exp Mech 1970:529–33.

[6] Kitaoka S, Mikuriya T. The effect of biaxial stress ratio on the propagation of mode I surface cracks by the combination of plane bending and cyclic torsion. Int J Fatigue 1996;18(3):205–11.

[7] Kitaoka S, Ono Y. The effect of second principal stress on the fatigue propagation of mode I surface crack in Al203/Al alloy composites. Int J Fatigue 2003;25:1347–55.

[8] Argence D, Weiss J, Pineau A. Observation and modelling of transgranular and intergranular multiaxial low-cycle fatigue damage of austenitic stainless steels. In: Proc. 4th Int. Conf. Biaxial/Multiaxial Fatigue, St. Germain en Laye, France, vol. 1, May 31–June 3, 1994, p. 309–322.

[9] Kullig E, Brückner-Foit A. Fracture mechanics assessment of planar branched cracks in equibiaxial stress field. Fat Fract Engng Mater Struct 1995;18(11):1277–88.

[10] Hoshide T, Socie DF. Crack nucleation and growth modelling in biaxial fatigue. Engng Fract Mech 1988;29(3):287–99.

[11] Maillot V, Fissolo A, Degallaix G, Degallaix S, Marini B, Le Roux JC. Initiation and growth of thermal fatigue crack networks in a 304 L type steel, In: Proc ECF14, Cracovie, 2002, p. 425–34.

[12] Seyedi M, Hild F, Taheri S. Crack propagation and shielding effects in a multicracked structure in thermal fatigue. In: Blom AF, editors. Proc Fatigue 2002, Stockholm, EMAS, vol.3, p. 1735–42.

[13] Angel T. Formation of martensite in austenitic stainless steels. J Iron Steel Inst 1954:165.

[14] Newman JC, Raju IS. Stress intensity factor equations for cracks in three-dimensional finite bodies. In: Lewis JC, Sines G, editors. Fracture mechanics, 14th Symposium. Theory and analysis ASTM STP 791, vol. I. Philadelphia: ASTM; 1983. p. 238–65.

[15] Song PS, Shieh YL. Crack growth and closure behaviour of surface cracks. Int J Fatigue 2004;26:429–36.

[16] Lange DA, Jennings HM, Shah SP. Analysis of surface-roughness using confocal microscopy. J Mater Sci 1993;28(14):3879–84.

[17] Bethge K, Munz D, Stamm H. Growth of semi-elliptical surface cracks in ferritic steel plates under cyclic thermal shock loading. Fat Fract Engng Mater Struct 1988;11(6):467–82.

[18] Chermahini RG, Palmberg B, Blom AF. Int J Fatigue 1993;15:259–63.

[19] Roychowdhury S, Dodds Jr RH. A numerical investigation of 3D small-scale yielding fatigue crack growth. Engng Fract Mech 2003;70:2363–83.

[20] Zhang JZ, Bowen P. On the finite element simulation of three dimensional semi-circular fatigue crack growth and closure. Engng Fract Mech 1998;60:341–60.

[21] Skinner JD, Daniewicz SR. Simulation of plasticity-induced fatigue crack closure in part-through cracked geometries using finite element analysis. Engng Fract Mech 2002;69:1–11.

[22] Ogura K, Ohji K, Honda K. Influence of mechanical factors on the fatigue crack closure, Fracture 1977. Advances in research on the strength and fracture of materials. In: Taplin DMR, editor. Proc. ICF4, Waterloo, vol. 2B. Pergamon; 1977. p. 1035–47.

[23] Fleck NA, Newman Jr JC. Analysis of crack closure under plane strain conditions. In: Newman Jr JC, Elber W, editors. Mechanics of fatigue crack closure. ASTM STP 982. ASTM; 1988. p. 319–41.

[24] Cotterell B, Rice JR. Slightly curved or kinked cracks. Int J Fract 1980;16:155–69.

[25] Wang X. Elastic T stress for semi-elliptical surface cracks in finite thickness plates. Engng Fract Mech 2003;70:731–56.

[26] Wang X, Bell R. Elastic T stress for semi-elliptical surface cracks in finite thickness plates subject to non-uniform stress distributions. Engng Fract Mech 2004;71:1477–96.

[27] Xu G, Bower AF, Ortiz M. An analysis of non-planar crack growth under mixed-mode loading. Int J Solids Struct 1994;31(16):2167–93.

[28] Mei Z, Morris JW. Influence of deformation-induced martensite on fatigue crack propagation in 304 stainless steels. Met Trans 1990;21A:3137–52.

[29] Mei Z, Morris Jr JW. Analysis of transformation-induced crack closure. Engng Fract Mech 1991;39(3):569–73.

[30] Stringfellow RG, Parks DM, Olson GB. A constitutive model for transformation plasticity accompanying strain-induced martensitic transformation in metastable austenitic steels. Acta Met Mat 1992;40(7):1703–16.

[31] Tomita Y, Iwamoto T. Computational prediction of deformation behavior of TRIP steels under cyclic loading. Int J Mech Sci 2001;43:2017–34.

[32] Isida M, Yoshida T, Noguchi H. Parallel array of semi-elliptic surface cracks in semi-infinite solid under tension. Engng Fract Mech 1991;39(5):845–50.
[33] Moes N, Dolbow J, Belytschko T. A finite element method for crack growth without remeshing. Int J Num Methods Engng 1999;46(1):131–50.
[34] Liang J, Huang R, Prevost JH, Suo Z. Evolving crack patterns in thin films with the extended finite element method. Int J Solids Struct 2003;40(10):2343–54.